7. Models to Explain Gravity Changes on Merapi Volcano

In the following chapter we assume, that the observed gravity changes are caused by mass migration below and/or above the surface of the volcano. Three processes are possible:

- ascending and descending of magma from the magma reservoir to the crater rim along faults inside the volcano's edifice. Thereby magma moves along open cracks and will be deposited as lava dome at the volcano's summit.
- magma is deposited as lava at the dome of the volcano. The surface topography of the summit is changing significantly causing gravity changes at stations near to the dome.
- changes of the groundwater levels around Merapi. The hydrothermal system is changing therefore. Meteoric water infiltrates in deeper layers. Such layers have been identified in a depth between 500 and 2000 m under Merapi (Müller et al., 1999) as layers with very low resistivity which can only be explained if all pores of the layers are filled with fluids.

Different geometric models have been developed and analyzed to explain gravity changes due to the different causes of mass migration unless gravity changes due to changes of summit topography which are not investigated because of missing topographic data.

A critical value in these models is the density of magma ρ_{magma}. ρ_{magma} at Merapi can change from 2000 kg/m^3 – 2900 kg/m^3 (Spieler, 1998). A good average value seems to be ρ_{magma} = 2400 kg/m^3 (Jousset, 1996).

7.1. Model 1: Sphere and Dipping Thin Pipe

In this model the magma migrates from a magma chamber in 8692.5 m depth below surface along an inclined, thin pipe up to the summit (fig. 7.4). The model was proposed by Beauducel and Cornet, (1999), based on the detailed analysis of tilt- and GPS-observations.

As parameters of the model the following values (Beauducel and Cornet, 1999) are introduced:

- radius of sphere r_{sphere} = 137 m
- radius of pipe r_{pipe} = 20 m
- length of pipe l_{pipe} = 8692.5 m
- inclination α of pipe to South-East= 103^o.092
- density of magma ρ_{magma} = 2400 kg/m^3
- density of surrounding material (marine sediments) $\rho_{sediment}$ = 2100 kg/m^3

The vertical gravitational effect of the magma ascending in the pipe to different levels was calculated using equations 4.2 for a inclined thin rod and 4.1 for a sphere for the stations at the crater rim JRA13, JRA15 and JRA100 (fig. 7.1). Significant gravity changes are obtained, if the magma comes near to the stations itself. Then the pipe is nearly filled with magma. Magma movements in the pipe in a depth > 1000 m generate small gravity changes which cannot become detected with conservative gravity observation techniques.

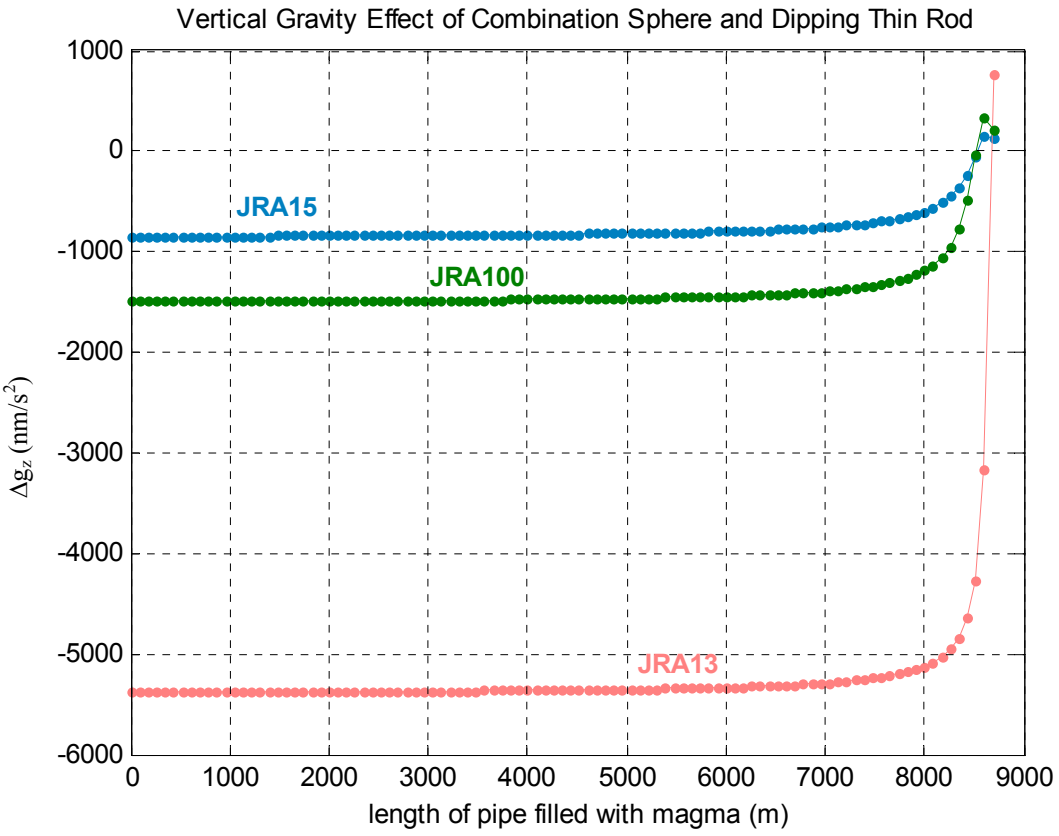

Fig.7.1. Vertical gravity effects (nm/s^2) of magma ascending in an inclined pipe of 20 m radius from the magma chamber at 0 m up to the surface at the stations JRA15, JRA13, and JRA100. The pipe reaches near to station JRA13 the surface.

Mass migration within the magma chamber causes also very small gravity changes, which are not observable at the surface. Observed gravity changes can be only explained by changes of the filling height of the pipe with magma near to the surface.

It is possible to generate contour line maps of the vertical gravity effects in the following way: the filling height of the pipe is calculated for the observed gravity change. At the x-axis the final height is mapped at the y-axis the height at the beginning, which is necessary to generate the observed gravity change. With such plots we can estimate in a graphical way the probable height changes of magma in the pipe from observation epoch to observation epoch. Fig. 7.2 shows the contour lines of gravity changes at stations JRA13 (767 ± 223 nm/s^2) and JRA15 (556 ± 219 nm/s^2) between campaigns IV (August 1999) and I (August 1997). The red-bold line is the value of gravity change at JRA13 (767 nm/s^2) and the red-thin lines are the value of gravity change ± standard deviation (990 = 767 + 223 nm/s^2 and 544 = 767 – 223 nm/s^2). The blue-bold line is the value of gravity change at JRA15 (556 nm/s^2) and the blue-thin lines are the value of gravity change ± standard deviation (775 = 556 + 219 nm/s^2 and 337 = 556 – 219 nm/s^2).

Fig. 7.3 shows the contour lines of gravity changes at station JRA13 (1787 ± 226 nm/s^2), JRA15 (1063 ± 222 nm/s^2), and JRA100 (741 ± 233 nm/s^2) between campaigns V (August 2000) and campaign I (August 1997).

The intersection of both contour lines in fig 7.2 and fig. 7.3 gives the position of magma L in the dipping thin rod. Table 7.1 shows the position of magma at the first campaign (August 1997) and second campaign (August 1999). Table 7.2 gives the position of magma between the first campaign (August 1997) and second campaign (August 2000) together with mean and standard deviation.

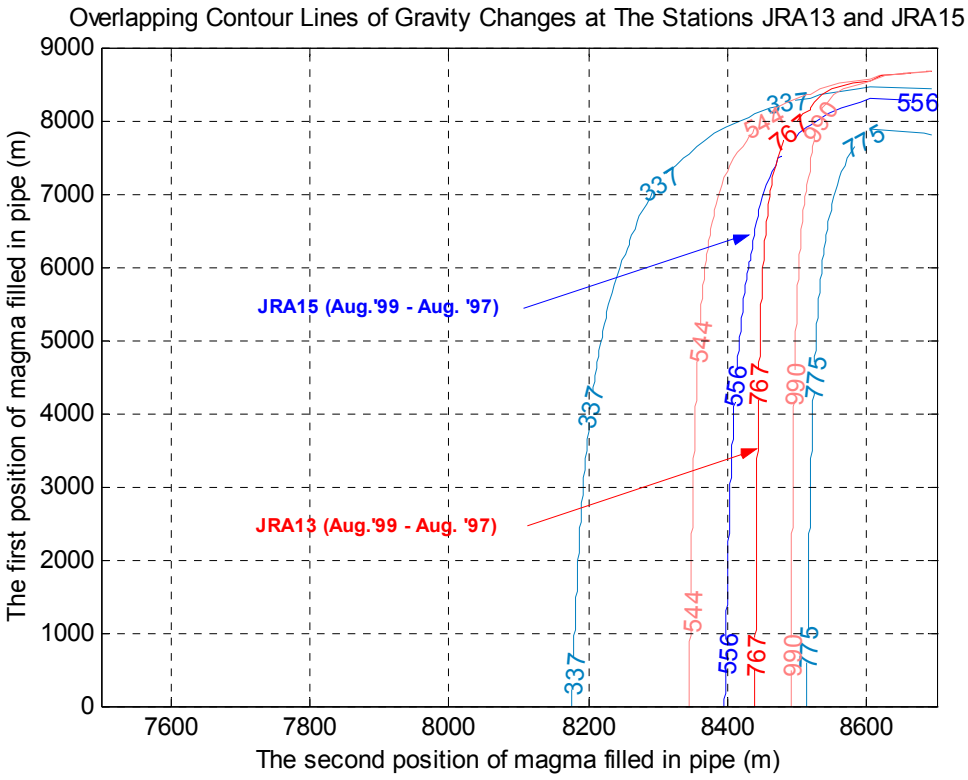

Fig.7.2. Height changes of magma in the pipe as deduced from gravity changes at stations JRA13 and JRA15 between August 1999 and August 1997 using the "sphere and dipping thin rod model".

Tab.7.1. Intersections of contour lines of gravity changes at stations JRA13 and JRA15 (from fig.7.2)

Length of pipe filled with magma (m)	
First position (August 1997)	Second position (August 1999)
7420	8470
8012	8530
8220	8479
8347	8535
8386	8559
8077 ± 395	8515 ± 38

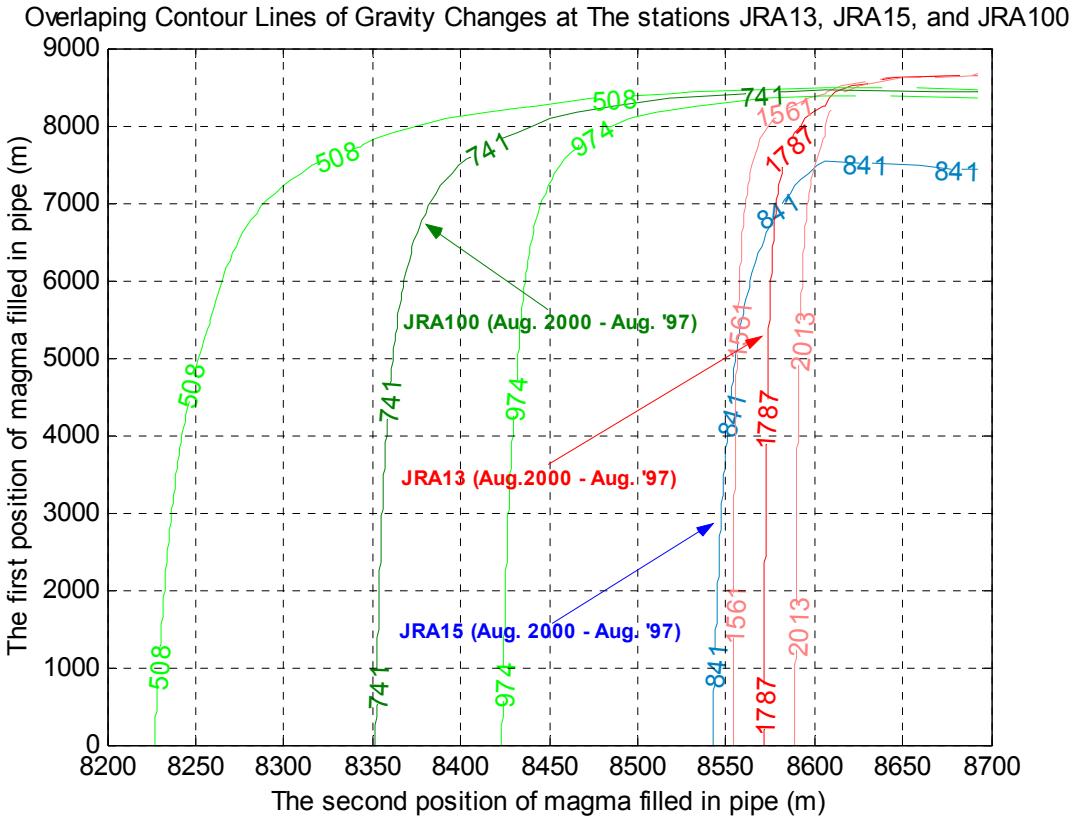

Fig.7.3. Height changes of magma in the pipe as deduced from gravity changes at stations JRA13, JRA15 and JRA100 between August 2000 and August 1997 using the "sphere and dipping thin rod model".

Tab.7.2. Intersections of contour lines of gravity changes at stations JRA13, JRA15 and JRA100 (from fig. 7.3).

Length of pipe filled with magma (m)	
First position (August 1997)	Second position (August 2000)
8385	8615
8387	8610
8386	8603
8446	8619
8447	8614
8449	8609
8471	8621
8472	8616
8474	8611
8435 ± 38	8613 ± 6

Fig. 7.4 shows the position estimation of magma at the dipping thin rod in August 1997, August 1999, and August 2000 based on the "sphere and dipping thin rod model".

The results of magma height for 1997 in table 7.1 and 7.2 are different; as mean value (8077 + 8435)/2 = 8256 m is obtained.

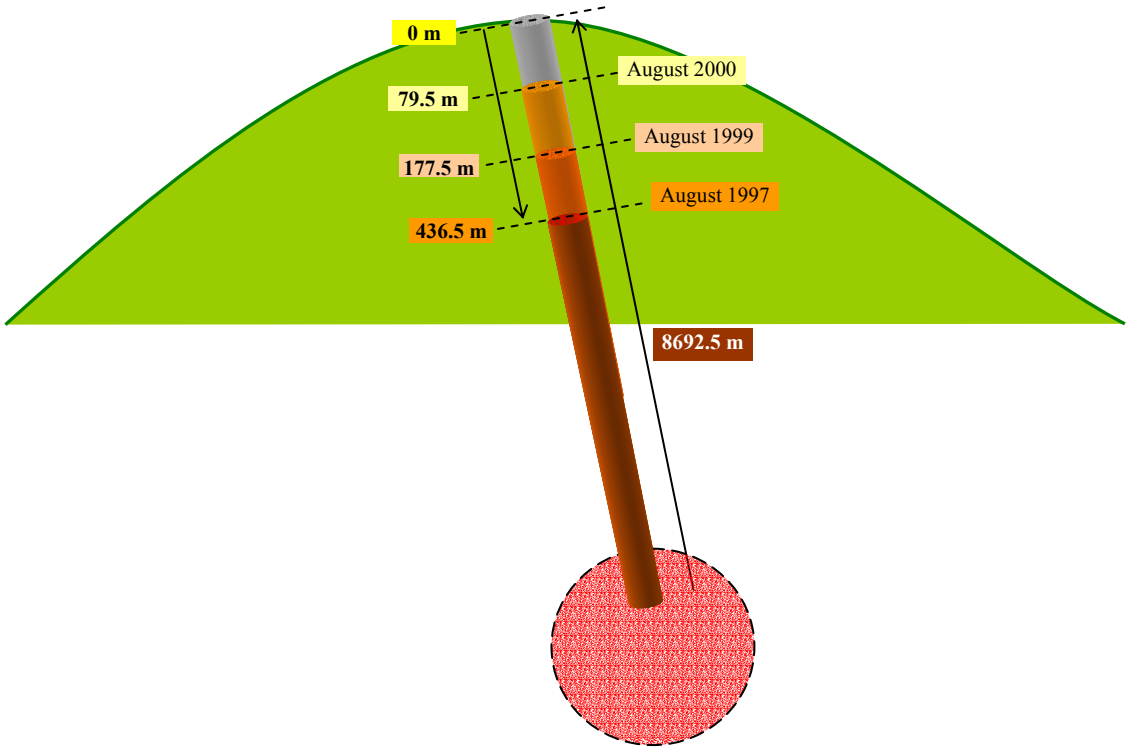

Fig.7.4. Magma height in the pipe of the “sphere and dipping thin rod model”.

7.2. Model 2: Sphere and Vertical Thin Pipe

A special situation is obtained if the thin rod is vertical. Similar to the "sphere and dipping thin rod model" (chapter 7.1), two parameters in this model are changing, i.e. pipe length = 8463 m and inclination (α) = 90°. Many results of the vertical gravity effect of the sphere and vertical thin rod model at the third loop, the profile along the north flank, the second loop, the first loop stations are presented in the chapter 7.2.1, 7.2.2, 7.2.3, and 7.2.4 respectively.

7.2.1. Vertical gravity effects at the third loop stations (top of Merapi > 2900 m)

Fig. 7.5 shows the vertical gravity effects (nm/s^2) at the stations JRA13, JRA15, and JRA100 as function of a vertical pipe filled with magma. The pipe is part of the "sphere and vertical thin rod model".

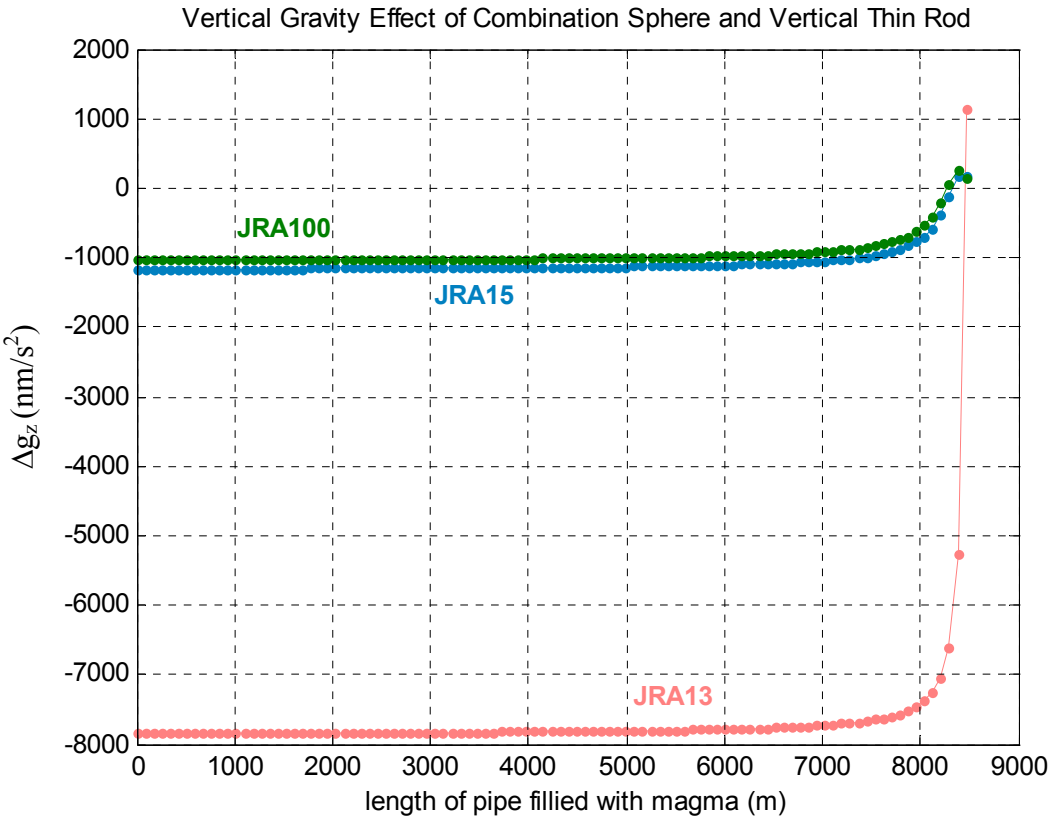

Fig.7.5. Vertical gravity effects (nm/s^2) at JRA13, JRA15, and JRA100 as function of a pipe (rod) filled with magma; the top of the rod reaches near JRAK13 the surface.

Fig. 7.6 shows the contour lines of gravity changes at the stations JRA13 (767 ± 223 nm/s^2) and JRA15 (556 ± 219 nm/s^2) between campaigns IV (August 1999) and I (August 1997); fig. 7.7 gives the contour lines of gravity changes at stations JRA13 (1787 ± 226 nm/s^2), JRA15 (1063 ± 222 nm/s^2), and JRA100 (741 ± 233 nm/s^2) between campaign V (August 2000) and I (August 1997). Table 7.3 lists the magma heights August 1997 and August 1999 as the intersections of contour lines; table 7.4 is the list of magma heights during August 1997 and August 2000 determined from many intersections of the contour lines in fig.7.7.

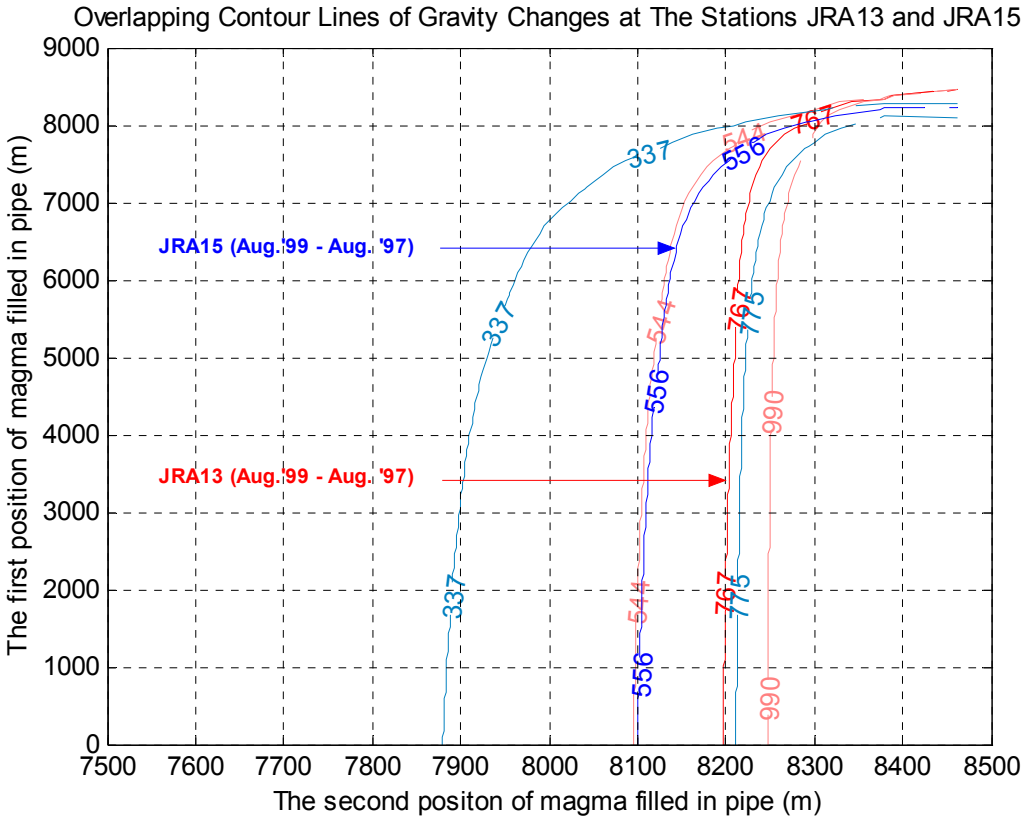

Fig.7.6. Height changes of magma in the pipe as deduced from gravity changes at stations JRA13 and JRA15 between August 1999 and August 1997 using the "sphere and vertical thin pipe model".

Tab.7.3. Intersections of contour lines of gravity changes at stations JRA13 and JRA15 (from fig. 7.6)

Magma height in pipe(m)	
August 1997	August 1999
7739	8295
8084	8295
8095	8313
8181	8296
8212	8316
8237	8338
8085 ± 184	8309 ± 17

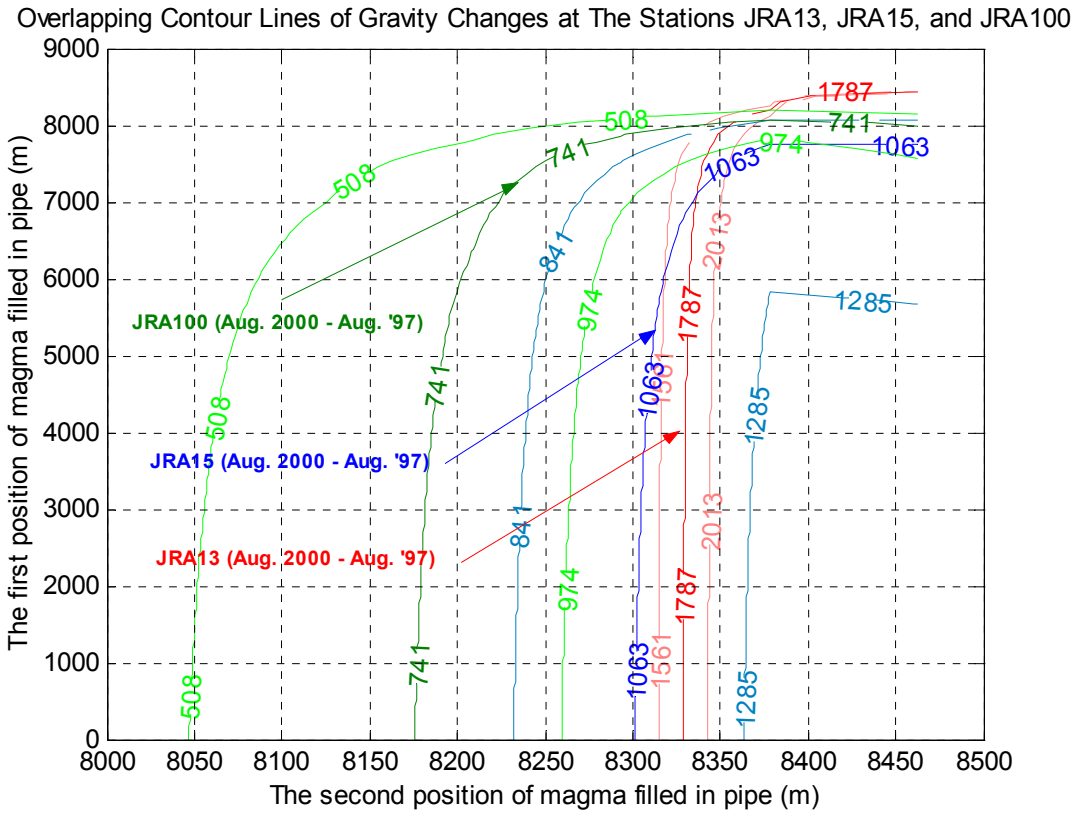

Fig.7.7. Height changes of magma in the pipe as deduced from gravity changes at stations JRA13, JRA15 and JRA100 between August 2000 and August 1997 using the "sphere and vertical thin pipe model".

Tab.7.4. Intersections of contour lines of gravity changes at stations JRA13, JRA15 and JRA100 (from fig.7.7).

Magma height (m)	
August 1997	August 2000
7891	8336
7976	8354
8042	8372
8007	8342
8045	8358
8073	8375
8006 ± 65	8356 ± 16

Fig. 7.8 shows the magma height in the vertical thin pipe (rod) in August 1997, August 1999, and August 2000 for the "sphere and vertical thin pipe model".

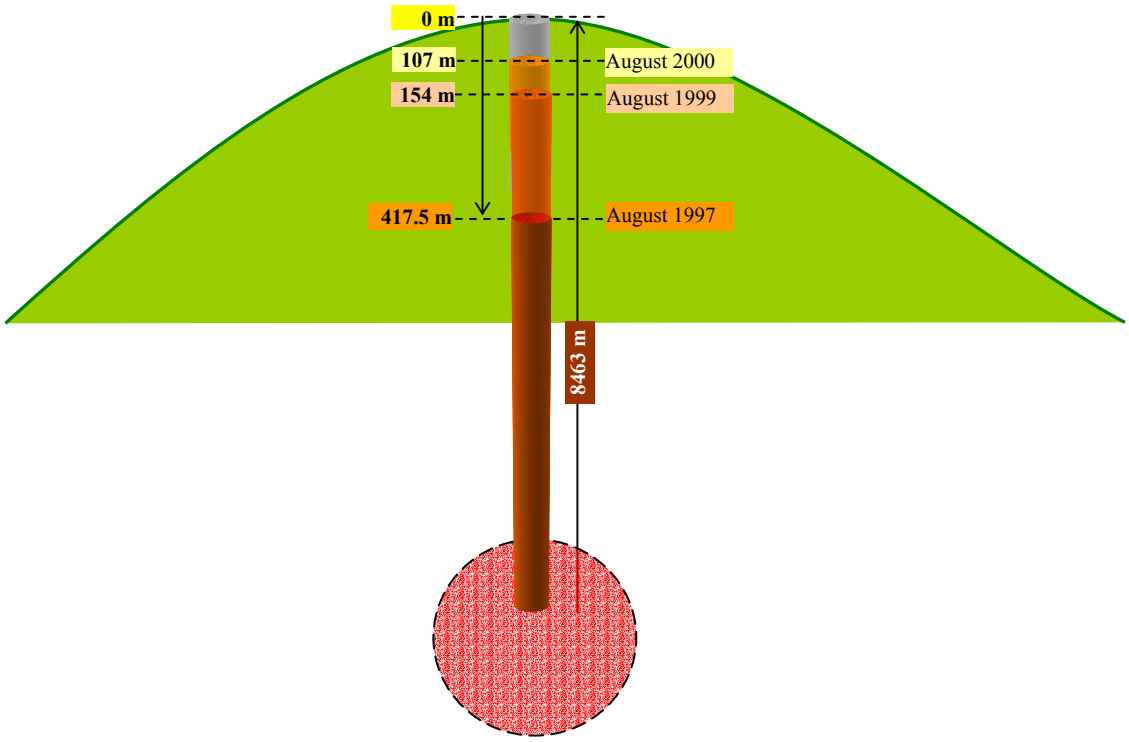

Fig.7.8. Magma height in the pipe of the "sphere and vertical thin pipe (rod) model".

7.2.2. Vertical gravity effects at the north flank

Fig. 7.9 shows the vertical gravity effects (nm/s^2) as function of a pipe filled with magma at the stations JRA1, JRA4, JRA6, and JRA9 of the "sphere and vertical thin rod model". Table 7.5 shows the values of vertical gravity effect at the stations JRA1, JRA4, JRA6, and JRA9, whereby the magma heights in fig. 7.8 for August 1997, August 1999, and August 2000 and are taken into account.

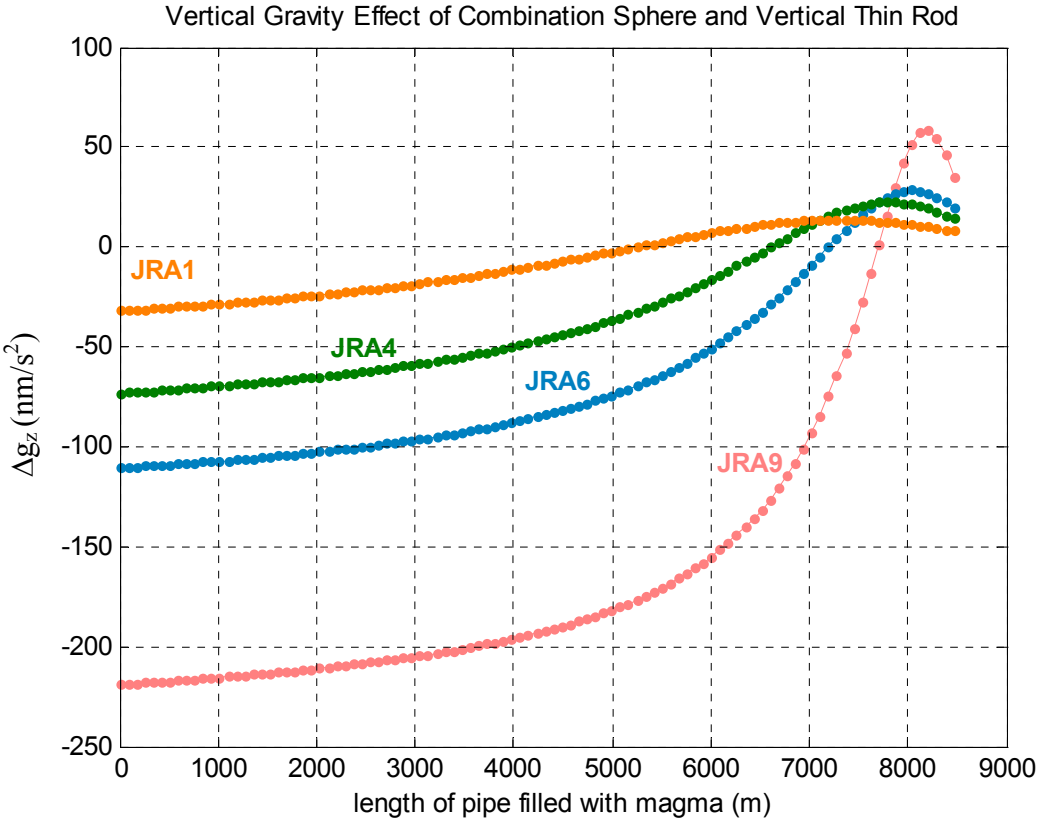

Fig.7.9. Vertical gravity effects (nm/s^2) of a vertical pipe filled with magma at JRA1, JRA4, JRA6, and JRA9; the top of rod reaches near JRAK13 the surface.

Tab.7.5. Vertical gravity effects (nm/s^2) of the "sphere and vertical thin rod model" at JRA1, JRA4, JRA6, and JRA9. Magma height is 8045.5 m (August 1997), 8305 m (August 1999) and 8356 m (August 2000).

	Vertical gravity effect of the sphere and vertical thin rod model				
Station	Aug. 1997	Aug. 1999	Aug. 2000	Aug. '99 – '97	Aug. 2000 – '97
	nm/s^2				
JRA1	11.23	9.45	9.06	-1.78	-2.17
JRA4	21.41	17.48	16.45	-3.57	-4.96
JRA6	28.45	24.64	23.11	-3.81	-5.34
JRA9	52.00	53.20	48.32	1.20	-3.68

7.2.3. Vertical gravity effects at the second loop stations (850 – 1500 m)

Fig. 7.10 shows the vertical gravity effect (nm/s^2) at the stations JRA0, BABA, MRIY, DELE, CEPO, and KALI as a function of the length of the pipe filled with magma. Table 7.6 gives the vertical gravity effect at the stations JRA0, BABA, MRIY, DELE, CEPO, and KALI considering the length of magma in the pipe in August 1997, August 1999, and August 2000 and their differences.

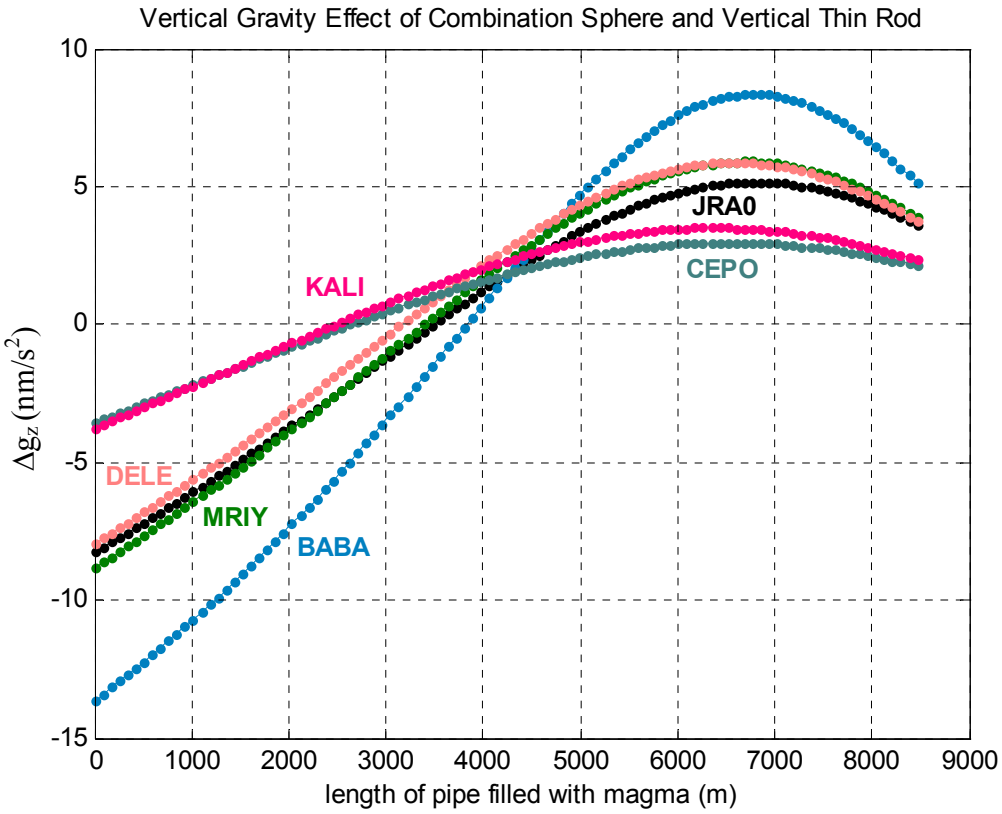

Fig.7.10. Vertical gravity effects (nm/s^2) of a vertical pipe filled with magma at JRA0, BABA, MRIY, DELE, CEPO, and KALI; the top of rod reaches near JRAK13 the surface.

Tab.7.6. Vertical gravity effects (nm/s^2) of the "sphere and vertical thin rod model" at JRA0, BABA, MRIY, DELE, CEPO, and KALI. Magma height is 8045.5 m (August 1997), 8305 m (August 1999) and 8356 m (August 2000).

	Vertical gravity effect of the sphere and vertical thin rod model				
Station	Aug. 1997	Aug. 1999	Aug. 2000	Aug. '99 – '97	Aug. 2000 – '97
	(nm/s^2)				
JRA0	4.28	3.89	3.81	-0.39	-0.47
BABA	6.44	5.65	5.48	-0.79	-0.96
MRIY	4.69	4.22	4.11	-0.47	-0.58
DELE	4.54	4.06	3.96	-0.48	-0.58
CEPO	2.44	2.25	2.21	-0.19	-0.23
KALI	2.74	2.50	2.45	-0.24	-0.29

7.2.4. Vertical gravity effects at the first loop stations (130 – 650m)

Fig. 7.10 shows the vertical gravity effects (nm/s^2) at the stations BUTU, MUNT, BOYO, and MVOY as a function of the magma height in the pipe. In table 7.7 the vertical gravity effects at the stations BUTU, MUNT, BOYO, and MVOY are listed using the model in fig. 7.8 for August 1997, August 1999, and August 2000 and their differences.

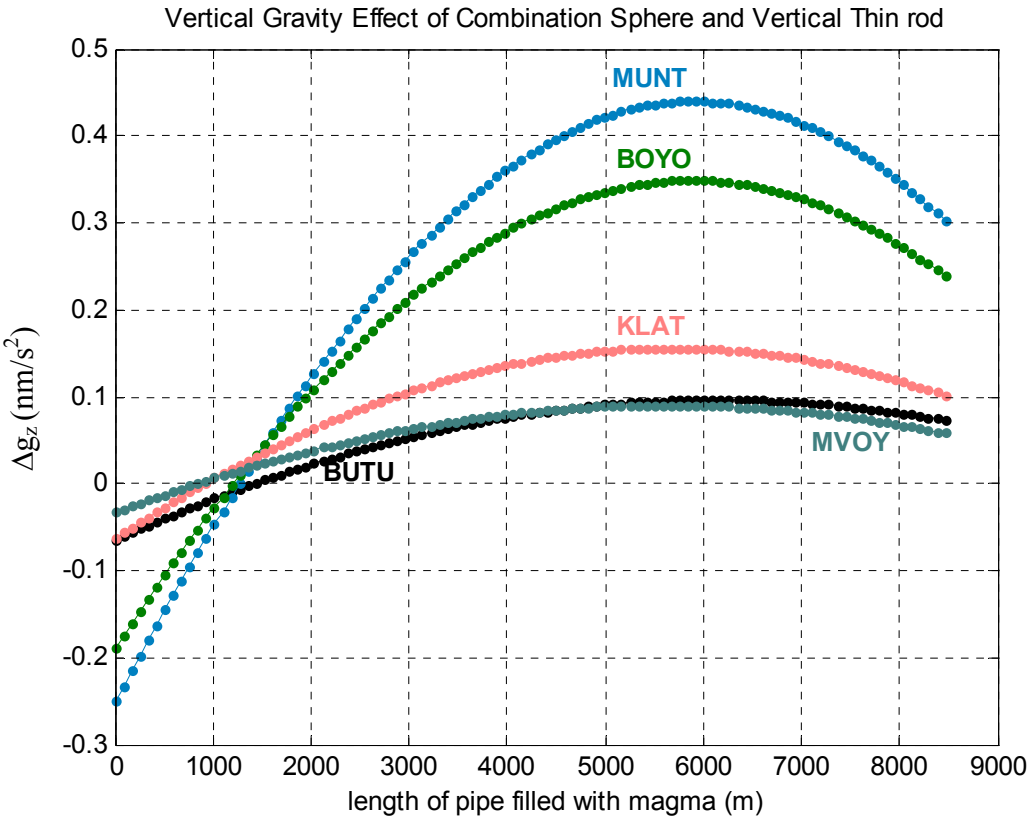

Fig.7.11. Vertical gravity effects (nm/s^2) of a vertical pipe filled with magma at BUTU, MUNT, BOYO, KLAT, and MVOY; the top of rod reaches near JRAK13 the surface.

Tab.7.7. Vertical gravity effects (nm/s^2) of the "sphere and vertical thin rod model" at BUTU, MUNT, BOYO, and MVOY. Magma height is 8045.5 m (Aug. 1997), 8305 m (Aug. 1999), and 8356 m (Aug. 2000).

	Vertical gravity effect of the sphere and vertical thin rod model				
Station	Aug. 1997	Aug. 1999	Aug. 2000	Aug. '99 – '97	Aug. 2000 – '97
	(nm/s^2)				
BUTU	0.08	0.08	0.07	0	-0.01
MUNT	0.34	0.32	0.31	-0.02	-0.03
BOYO	0.27	0.25	0.25	-0.02	-0.02
KLAT	0.12	0.11	0.11	-0.01	-0.01
MVOY	0.07	0.06	0.06	-0.01	-0.01

The vertical gravity effects of this model at the north flank, second and first loop stations are much smaller than the observed gravity changes (tab.6.2). We can conclude that the gravity changes at these stations cannot be explained by filling a sphere and a vertical thin rod with magma. Therefore another model to explain the observed gravity changes at these stations will be presented in chapter 7.4.

7.3. Model 3: Sphere and Vertical Thick Cylinder

Another three dimensional model is obtained if we replace the thin vertical rod by a thick vertical cylinder (equation 4.16). The results of the vertical gravity effect of the sphere and vertical thick cylinder model at the third loop, north flank, the second loop and the first loop stations are discussed in the chapters 7.3.1, 7.3.2, 7.3.3, and 7.3.4 respectively.

7.3.1. Vertical gravity effects at the third loop stations (top of Merapi > 2900 m)

Fig. 7.12 shows the vertical gravity effects (nm/s^2) at the stations JRA13, JRA15, and JRA100 as function of the height of magma in the cylinder for the "sphere and vertical thick cylinder model".

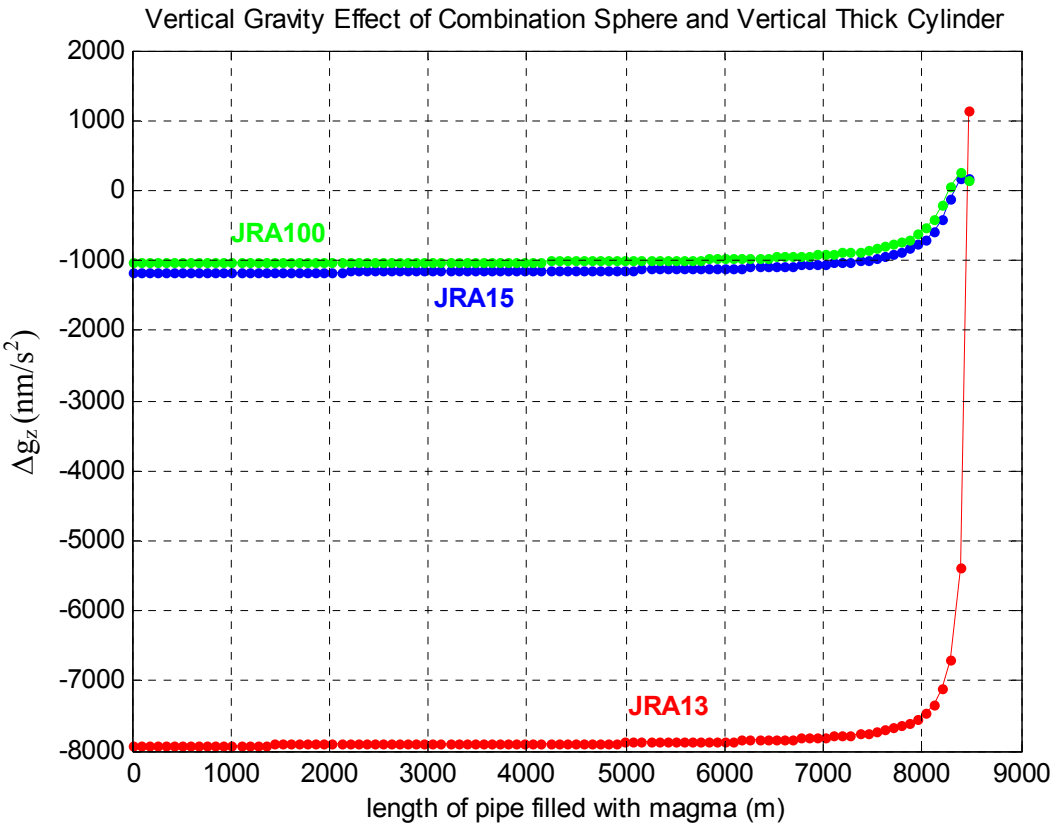

Fig.7.12. Vertical gravity effects (nm/s^2) at JRA13, JRA15 and JRA100 as function of magma height in the cylinder; the top of cylinder reaches near JRAK13 the surface.

In fig. 7.13 the contour lines of gravity changes at the stations JRA13 (767 ± 223 nm/s^2) and JRA15 (556 ± 219 nm/s^2) between campaigns IV (August 1999) and I (August 1997) are plotted. Fig. 7.14 presents the contour lines of gravity changes at station JRA13 (1787 ± 226 nm/s^2), JRA15 (1063 ± 222 nm/s^2), and JRA100 (741 ± 233 nm/s^2) for the campaigns V (August 2000) and I (August 1997). Magma heights changes are determined as the intersections of contour lines. Tables 7.8 and 7.9 list the magma heights in the cylinder for campaigns I (August 1997) and IV (August 1999) respectively for campaigns I and V (August 2000).

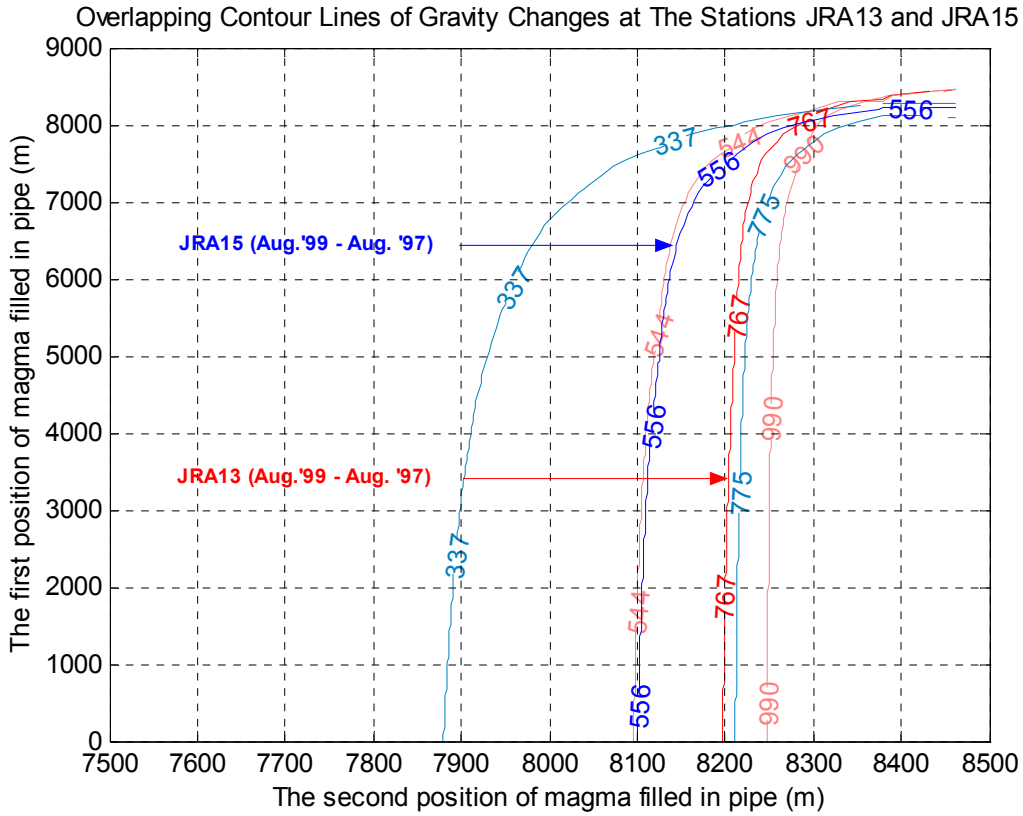

Fig.7.13. Height changes of magma in the cylinder as deduced from gravity changes at stations JRA13 and JRA15 between August 1999 and August 1997 using the "sphere and vertical thick cylinder model".

Tab.7.8. Intersections of contour lines of gravity changes at the stations JRA13 and JRA15 (from fig.7.13).

Magma heights in the cylinder (m)	
August 1997	August 1999
7741	8295
8049	8295
8098	8314
8182	8297
8214	8317
8240	8317
8087 ± 184	8310 ± 17

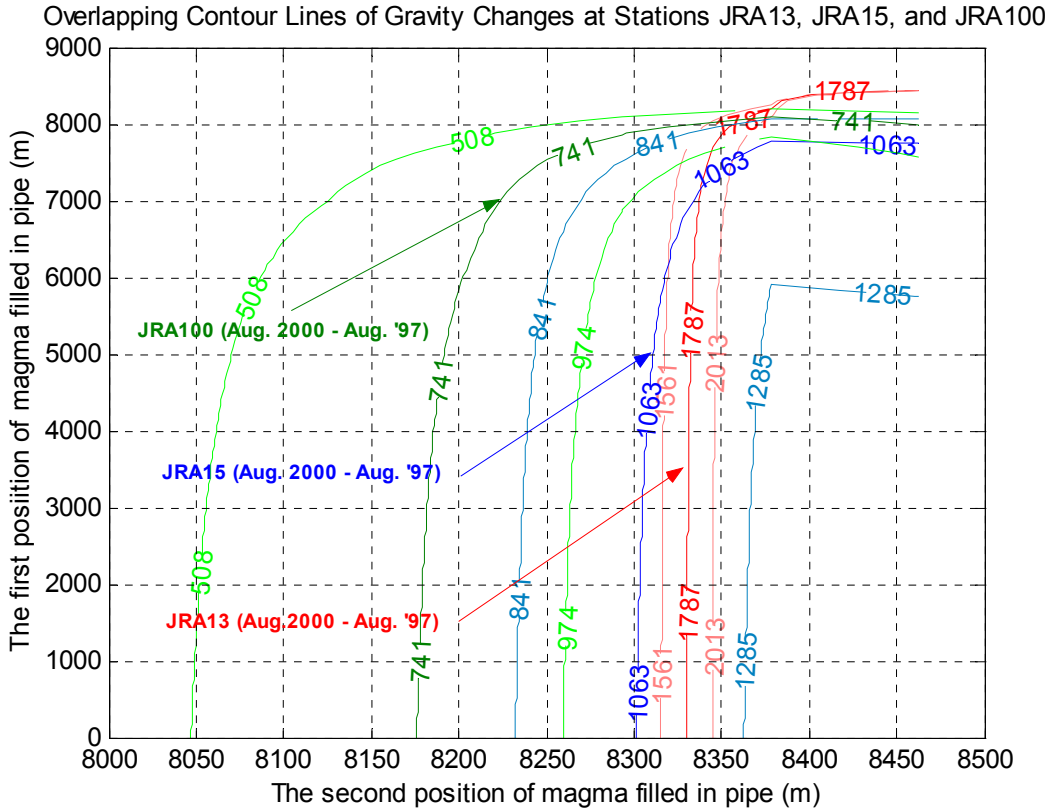

Fig.7.14. Height changes of magma in the cylinder as deduced from gravity changes at JRA13, JRA15, and JRA100 between August 2000 and August 1997 using the "sphere and vertical thick cylinder model"...

Tab.7.9. Intersections of contour lines of gravity changes at the stations JRA13, JRA15, and JRA100 (from fig. 7.14).

Magma heights in the cylinder (m)	
August 1997	August 2000
7902	8337
7987	8356
8053	8375
8013	8343
8051	8361
8080	8378
8014 ± 64	8358± 17

Fig. 7.15 shows the magma heights in the conduit in August 1997, August 1999, and August 2000 estimated with the "sphere and vertical thick cylinder model".

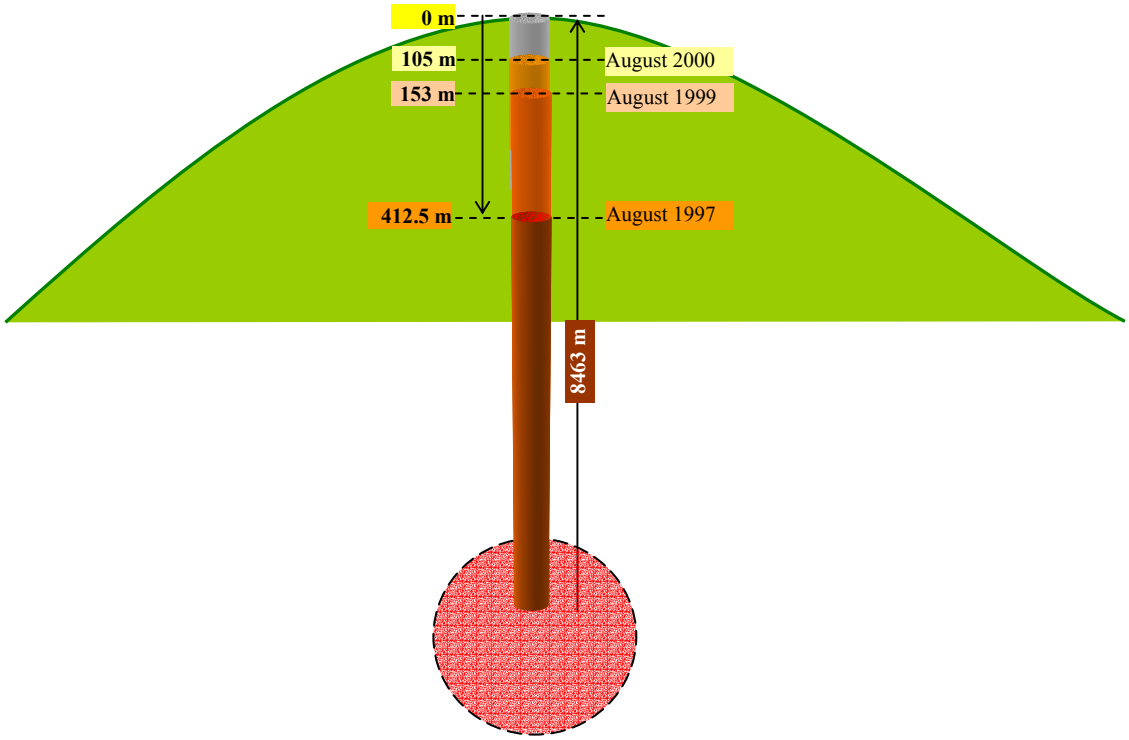

Fig.7.15. Magma height in the pipe of the "sphere and vertical thick cylinder model".

The position of magma in the pipe of the "sphere and vertical thin rod model" (fig. 7.8) is similar to the magma heights of the "sphere and vertical thick cylinder model".

7.3.2 Vertical gravity effects at the north flank

Fig. 7.16 shows the vertical gravity effects (nm/s^2) at the north flank stations JRA1, JRA4, JRA6, and JRA9 dependent on the magma height in the cylinder of the "sphere and vertical thick cylinder model". In table 7.10 the vertical gravity effects at the stations JRA1, JRA4, JRA6, and JRA9 are listed using the model in fig. 7.15 for August 1997, August 1999, and August 2000 and the differences between them.

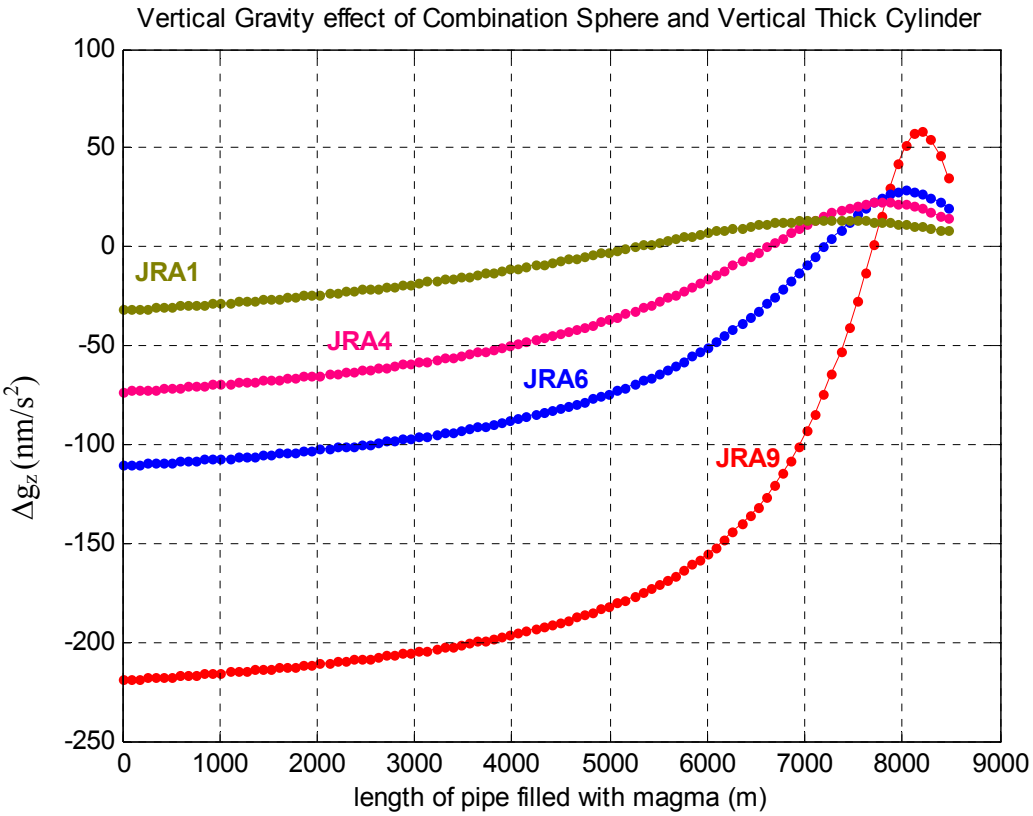

Fig.7.16. Vertical gravity effects (nm/s^2) as function of magma heights in the cylinder at JRA1, JRA4, JRA6 and JRA9; the top of the cylinder reaches near JRAK13 the surface.

Tab.7.10. Vertical gravity effects (nm/s^2) of the "sphere and vertical thick cylinder model" at JRA1, JRA4, JRA6, JRA9; as magma heights in the cylinder 8050.5 m (Aug. 1997), 8310 m (Aug. 1999), and 8358 m (Aug. 2000) are assumed (see tables 7.8 and 7.9).

	Vertical gravity effects of the sphere and vertical thick cylinder model				
Station	Aug. 1997	Aug. 1999	Aug. 2000	Aug. '99 – '97	Aug. 2000 – '97
	nm/s^2				
JRA1	11.19	9.41	9.04	-1.78	-2.15
JRA4	21.35	17.38	16.41	-3.97	-4.94
JRA6	28.43	24.49	23.05	-3.44	-5.38
JRA9	52.31	52.74	48.15	0.43	-4.16

7.3.3. Vertical gravity effects at the second loop stations (850 – 1500 m)

Fig. 7.17 presents the vertical gravity effects (nm/s^2) at the stations JRA0, BABA, MRIY, DELE, CEPO, and KALI as function of magma heights in the cylinder for the "sphere and vertical thick cylinder model". Table 7.11 shows the vertical gravity effects at the stations JRA0, BABA, MRIY, DELE, CEPO, and KALI using the magma heights given in fig. 7.15 in August 1997, August 1999, and August 2000 and the differences between them.

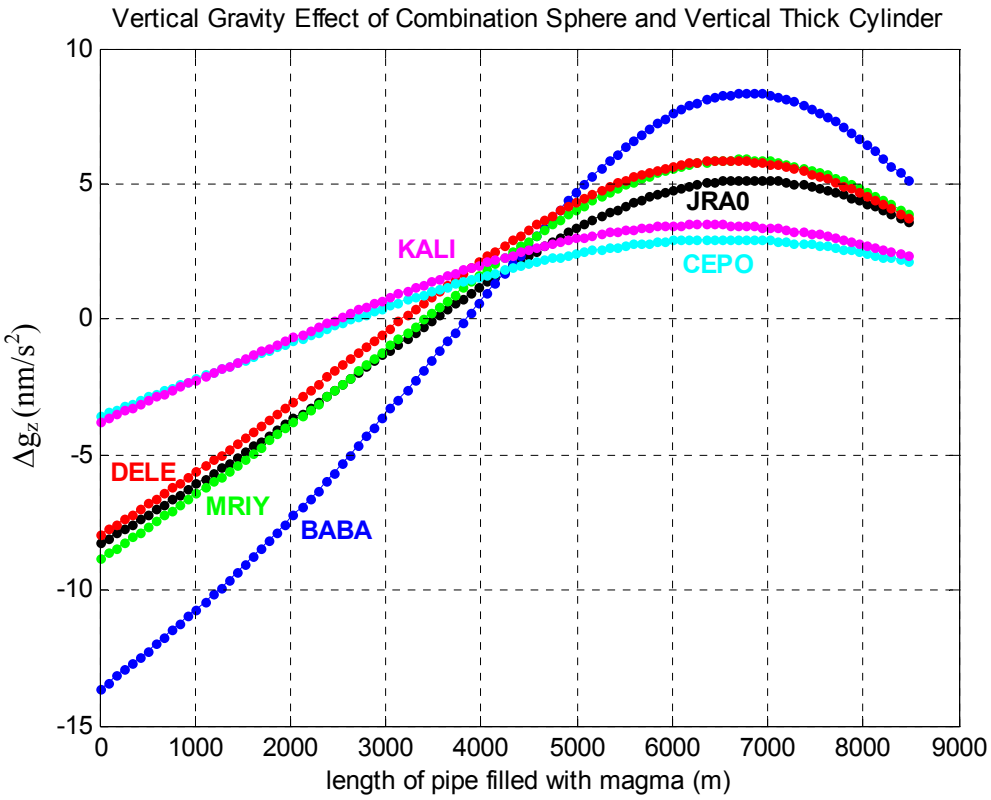

Fig.7.17. Vertical gravity effects (nm/s^2) as function of magma heights in the cylinder at JRA0, BABA, MRIY, DELE, CEPO, and KALI; the top of the cylinder reaches near JRAK13 the surface.

Tab.7.11. Vertical gravity effects (nm/s^2) of the "sphere and vertical thick cylinder model" at the stations JRA0, BABA, MRIY, DELE, CEPO, and KALI; the magma heights in the cylinder are 8050.5 m (Aug. 1997), 8310 m (Aug. 1999), and 8358 m (Aug. 2000).

	Vertical gravity effect of the sphere and vertical thick cylinder model				
Station	Aug. 1997	Aug. 1999	Aug. 2000	Aug. '99 – '97	Aug. 2000 – '97
	nm/s^2				
JRA0	4.27	3.88	3.80	-0.39	-0.47
BABA	6.43	5.63	5.47	-0.80	-0.96
MRIY	4.69	4.21	4.11	-0.48	-0.58
DELE	4.53	4.05	3.96	-0.48	-0.57
CEPO	2.43	2.25	2.21	-0.18	-0.22
KALI	2.74	2.49	2.45	-0.25	-0.29

7.3.4. Vertical gravity effects at the first loop stations (130 – 650m)

Fig. 7.18 shows the vertical gravity effects (nm/s^2) at the stations BUTU, MUNT, BOYO, and MVOY as a function of magma height in the cylinder of the "sphere and vertical thick cylinder model". In table 7.12 the vertical gravity effects at these stations and their differences are listed.

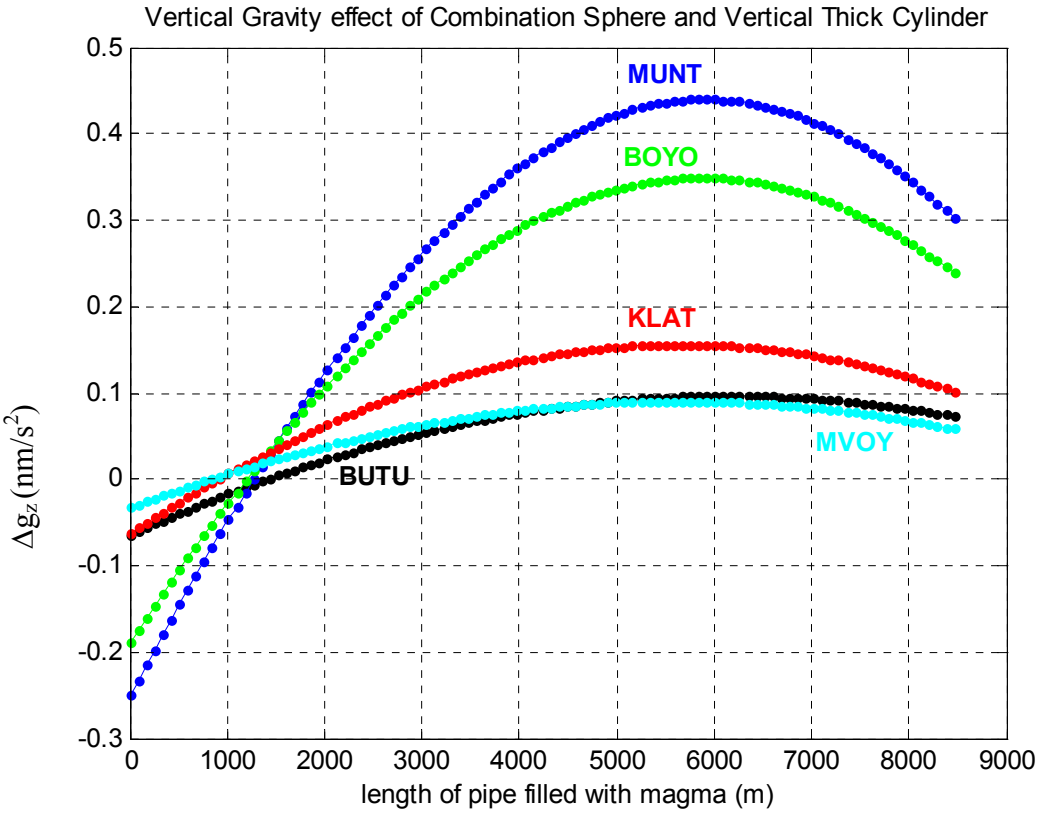

Fig.7.18. Vertical gravity effects (nm/s^2) as function of magma heights in the cylinder at the stations BUTU, MUNT, BOYO, KLAT, and MVOY; the top of the cylinder reaches near JRAK13 the surface.

Tab.7.12. Vertical gravity effects (nm/s^2) of the "sphere and vertical thick cylinder model" at the stations BUTU, MUNT, BOYO, KLAT and MVOY; the magma heights in the cylinder are 8050.5 m (Aug. 1997), 8310 m (Aug. 1999), and 8358 m (Aug. 2000).

	Vertical gravity effect of the sphere and vertical thick cylinder model				
Station	Aug. 1997	Aug. 1999	Aug. 2000	Aug. '99 – '97	Aug. 2000 – '97
	nm/s^2				
BUTU	0.08	0.08	0.07	0	-0.01
MUNT	0.34	0.32	0.31	-0.02	-0.03
BOYO	0.27	0.25	0.25	-0.02	-0.02
KLAT	0.12	0.11	0.11	-0.01	-0.01
MVOY	0.07	0.06	0.06	-0.01	-0.01

The vertical gravity effects in tables 7.5, 7.6 and 7.7 are very similar to the values in tables 7.10, 7.11 and 7.12. Also the "sphere and vertical thick cylinder model" cannot explain the observed vertical gravity changes of the first and second loop.

7.4. Modeling of Water Table Changes

The observed gravity changes (table 6.2) at the stations of the north flank profile, second loop and first loop are much bigger than the results of model computation presented in the previous chapters. On the other side LOTEM and resistivity observations suppose the existence of subsurface layers saturated with low resistance fluids as shown in fig. 7.19a.

Based on the formulas in the chapter 4.2.3, a model consisting of 10 concentric, vertical cylinders with different densities was constructed. The vertical axes of the cylinders are located at the summit of Merapi Volcano (fig. 7.19b and 7.19c). The geometric parameters of the cylinders (inner-radius R_{in} , outer-radius R_{out} and length L) are listed in table 7.13. The vertical gravity effects for each cylinder at particular stations are calculated by equation 4.16. The name of the program is concentric_cyl.m.

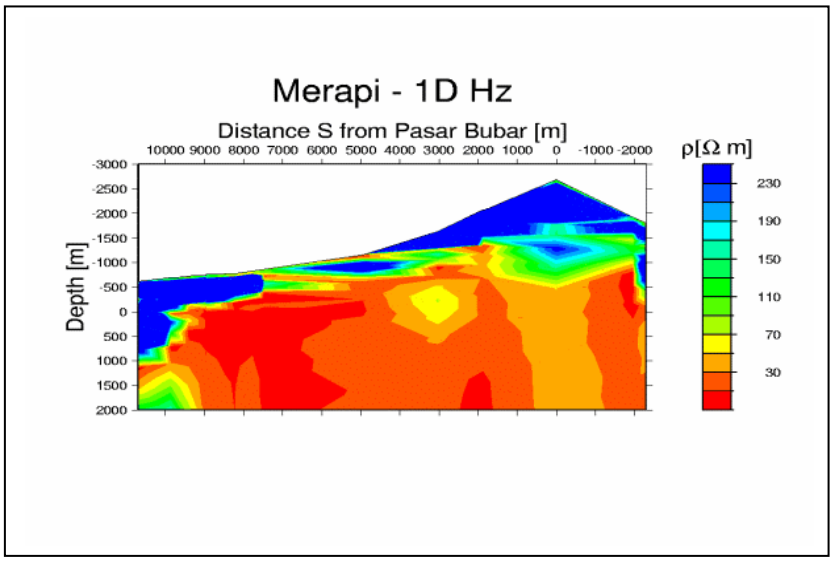

Fig. 7.19.a. Plot of the resistivity distribution and the topography on the north-south-profile. Red: low resistivity; Blue: high resistivity. Clearly notable are the high surface resistivities, e.g. below the summit (http://www.uni-koeln.de).

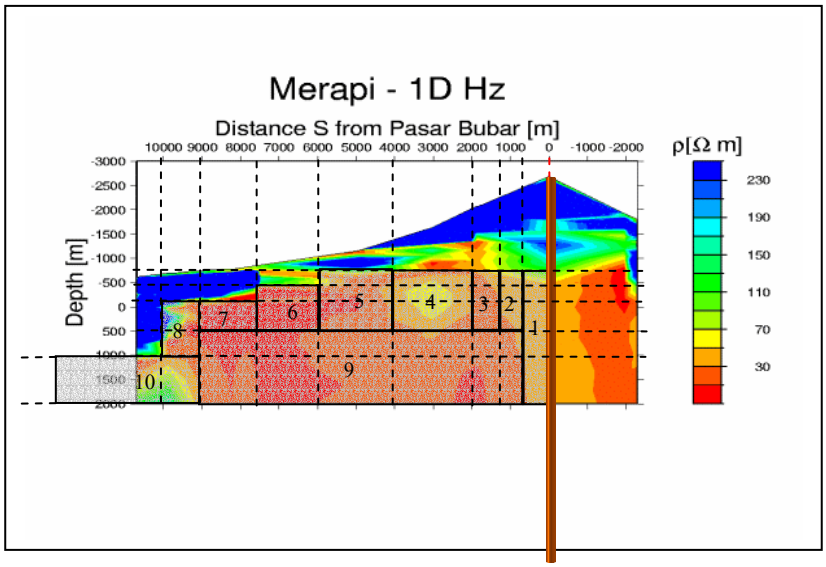

Fig. 7.19.b. Model of 10 concentric cylinders with the axes at the summit of Merapi volcano representing different resitivities structures.

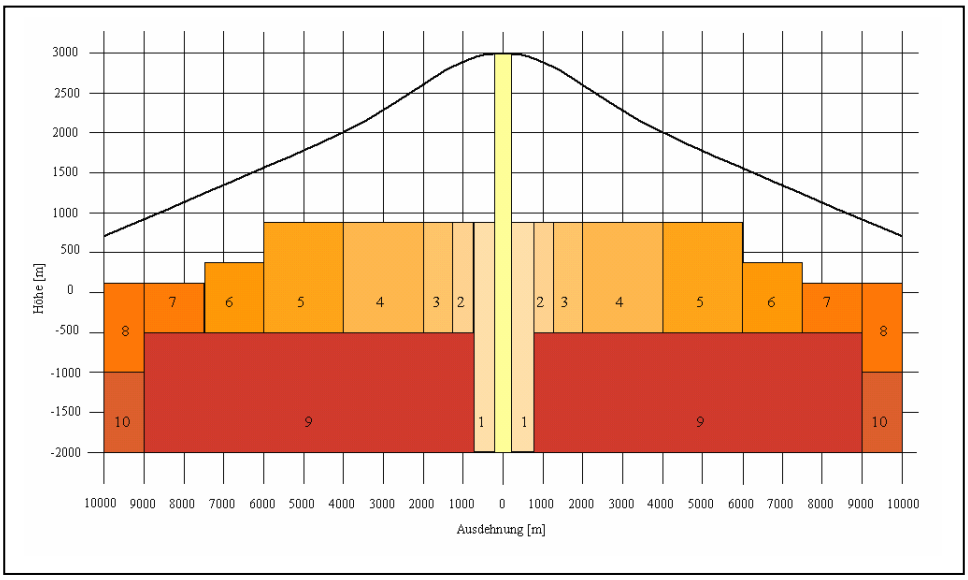

Fig. 7.19.c. Geometric size of the concentric cylinders (Held, 2002).

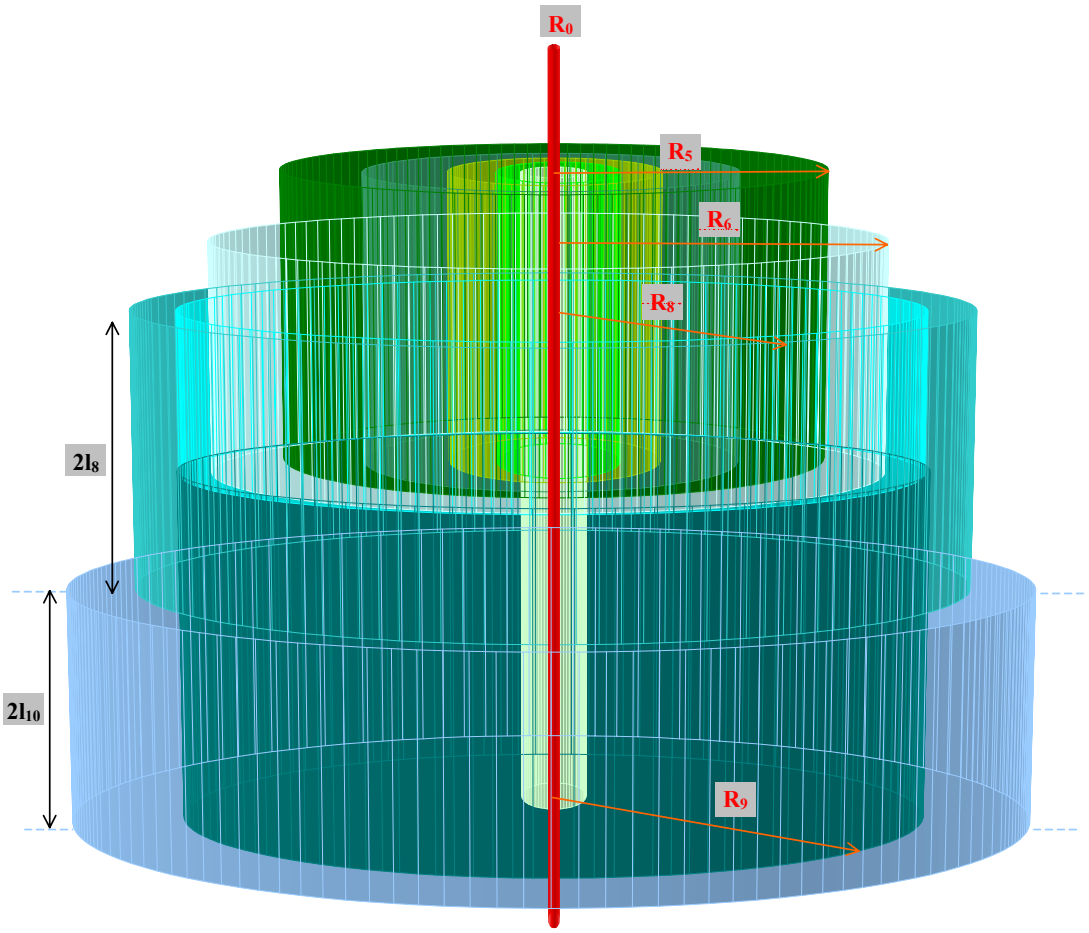

Fig. 7.19.d. Three dimensional view of the concentric cylinder model.

Tab. 7.13. Inner- and outer-radius of cylinders.

Cylinder	R_{out} (m)	R_{in} (m)	L (m)
1	750	20	2750
2	1250	750	1250
3	2000	1250	1250
4	4000	2000	1250
5	6000	4000	1250
6	7500	6000	1000
7	9000	7500	700
8	10000	9000	1200
9	9000	750	1500
10	30000	9000	1000

The density changes of each cylinder are determined by constraint linear least squares (chapter 4.2.3); the name of the program used is optim_density.m. As lower and upper constraints density changes of ±50 kg/m^3 are introduced.
Table 7.14 shows the results of density changes of each cylinder at campaigns Feb. 1998 – Aug. 1997, Aug.1998 – Aug. 1997, Aug.1999 – Aug. 1997, Aug. 2000 – Aug. 1997.

Tab. 7.14. Density changes of the concentric cylinders between August 1997, August 1998, August 1999 and August 2000; as constraints density changes of ±50 kg/m^3 are introduced.

	Density changes (kg/m^3)			
Cylinder	Feb. '98-Aug. '97	Aug. '98-Aug. '97	Aug. '99-Aug. '97	Aug. 2000-Aug. '97
1	-7.9	0.0	0.0	0.0
2	0.0	0.3	0.0	0.0
3	0.0	8.5	2.6	17.7
4	0.0	0.0	1.1	0.0
5	-1.2	0.3	0.2	0.0
6	0.0	0.0	0.0	0.0
7	0.0	4.3	2.7	2.3
8	0.0	0.0	0.0	0.0
9	0.0	0.0	0.0	0.0
10	-0.5	0.0	-0.2	-1.4

Fig. 7.20 a, b, c, d show the observed and modeled gravity changes between the particular campaigns.

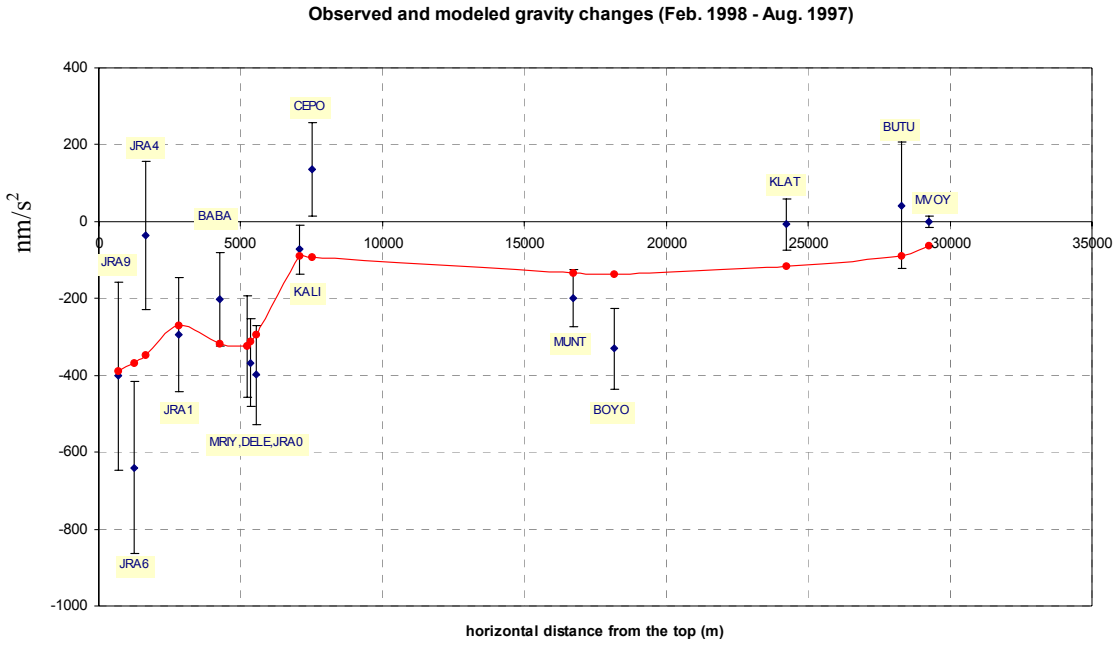

Fig. 7.20a. Observed (blue points and 2σ error bars) and modeled (red points and line) gravity changes between campaigns I (August 1997) and II (February 1998); as constraints density changes of ±50 kg/m^3 are introduced.

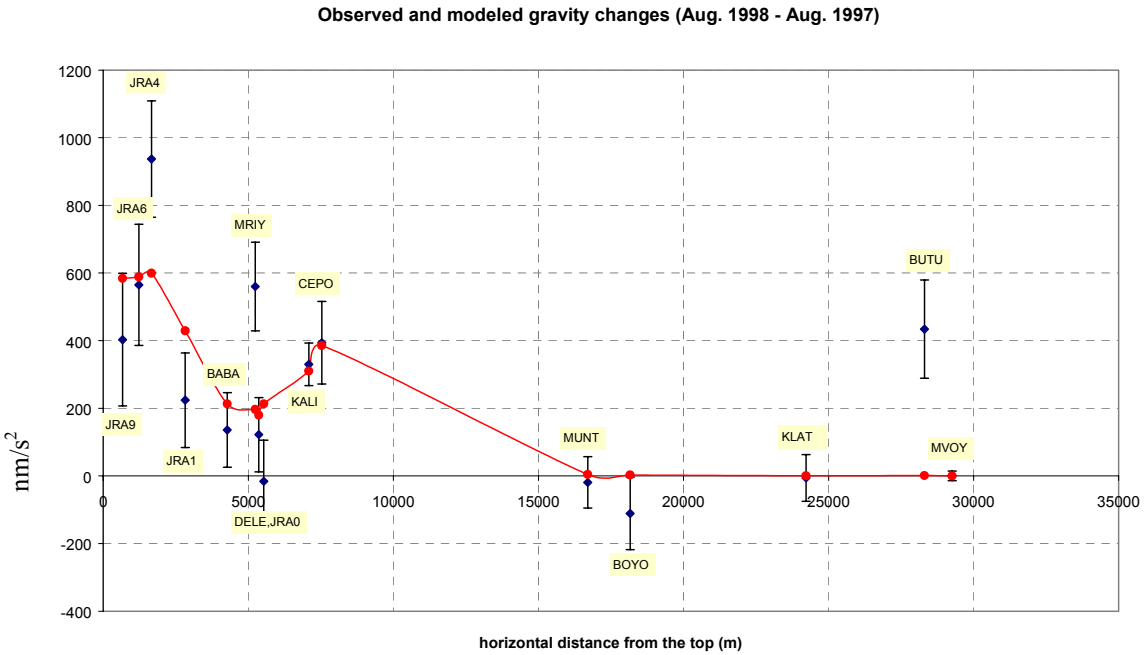

Fig. 7.20b. Observed (blue points and 2σ error bars) and modeled (red points and line) gravity changes between campaigns I (August 1997) and II (August 1998); as constraints density changes of ±50 kg/m^3 are introduced.

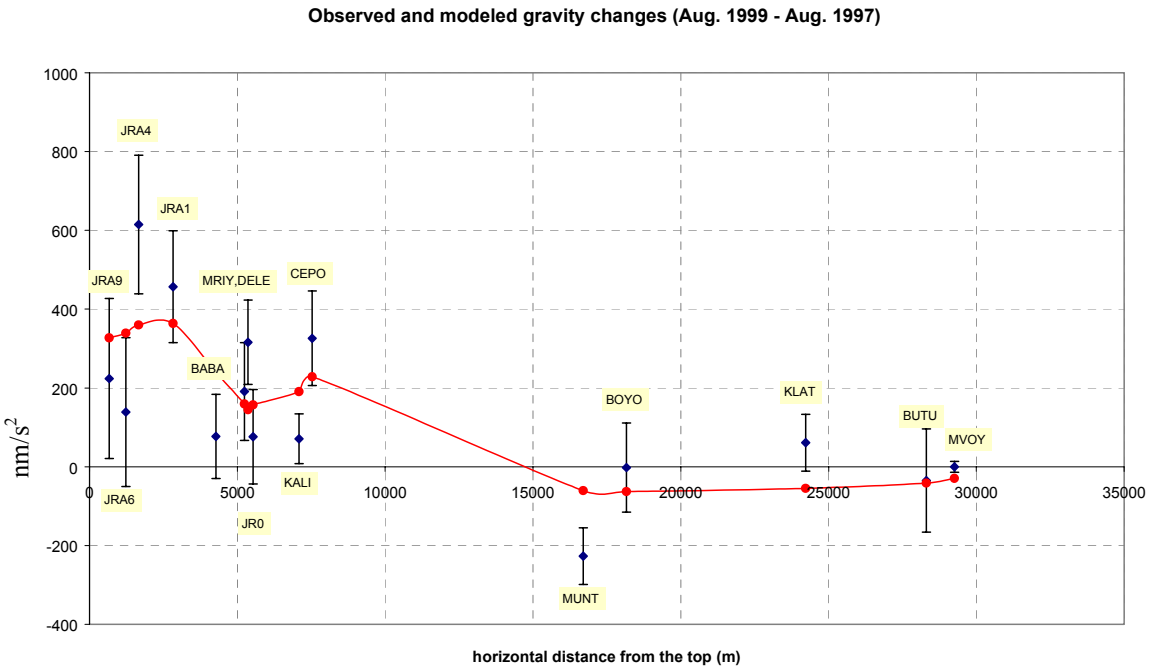

Fig. 7.20c. . Observed (blue points and 2σ error bars) and modeled (red points and line) gravity changes between campaigns I (August 1997) and II (August 1999); as constraints density changes of ±50 kg/m^3 are introduced

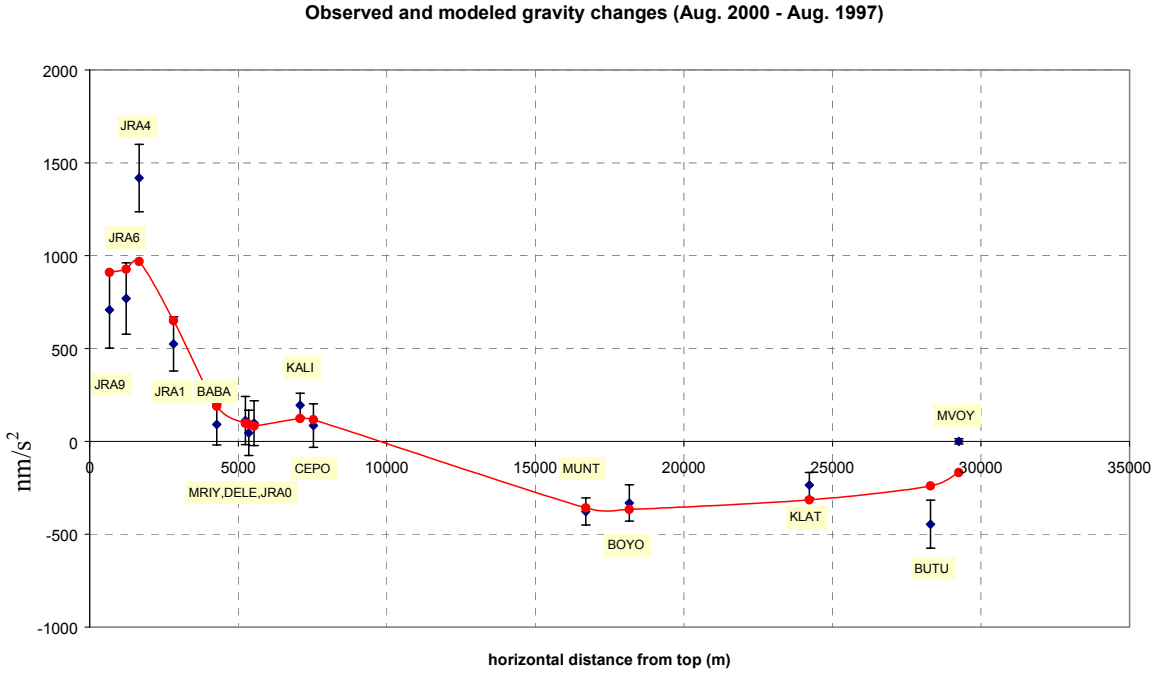

Fig. 7.20d. . Observed (blue points and 2σ error bars) and modeled (red points and line) gravity changes between campaigns I (August 1997) and II (August 2000); as constraints density changes of ±50 kg/m^3 are introduced.